Check for updates

Circularly polarized luminescence and nonlinear optical harmonic generation based on chiral zinc halides†

Xiao Han,[a] Puxin Cheng,[a] Wenqing Han,[a] Rongchao Shi,[a] Junjie Guan,[a] Geng Li[b] and Jialiang Xu ✱[a]

Chiral hybrid metal halides have grabbed extensive attention in linear and nonlinear chiroptics. Herein, 0D chiral zinc halides, (*R*-/*S*-2-MP)ZnCl₄, have been fabricated, which demonstrate high efficiency second-order nonlinear optical responses. Incorporating Sb³⁺ into the chiral zinc halide matrix triggers the circularly polarized luminescence effectively with a balance between quantum yield and luminescence dissymmetry factor.

Chiral materials possess a plethora of distinctive properties, stemming from their inherent asymmetry, particularly their capability to rotate the polarization of light.[1] Consequently, chiral materials have flourished in various research fields such as catalysis,[2] molecular recognition,[3] optics,[4,5] and magnetics,[6] *etc.*[7] Hybrid organic-inorganic metal halides (HOMHs) have been regarded as ideal candidates for the next-generation semiconductor materials in virtue of their facile solution-process syntheses, tuneable bandgaps, large exciton binding energies, and high optical-absorption coefficient.[8] Importantly, when compared to all-inorganic metal halides, the organic cations at the A site offer a greater abundance of diversity and substitutability. This has led to a significant expansion in the architecture of HOMHs, including the formation of low-dimensional polynuclear metal clusters, which in turn further broadens their potential applications in optoelectronics.[9]

Chiral metal halides combine the merits of chiral materials and HOMHs.[10] It has been also certificated that the chirality of chiral organic ligands can be conveyed to the inorganic scaffolds in metal halides.[11] Since Billing *et al.* reported the chiral lead-

a School of Materials Science and Engineering, Smart Sensing Interdisciplinary Science Center, Collaborative Innovation Center of Chemical Science and Engineering (Tianjin), Nankai University, Tongyan Road 38, Tianjin 300350, P. R. China. E-mail: jialiang.xu@nankai.edu.cn

b National Supercomputer Center in Tianjin, Tianjin 300457, China

based halides, *i.e.*, (*S*-β-phenethylammonium)PbBr₃,[12] various constructions among chiral metal halides, including 2D, quasi 2D, 1D, and 0D, have sprung up in the past decade. Chiral metal halides currently represent a crucial division of hybrid organic-inorganic materials.[13,14] On the one hand, the transfer of chirality from organic components eliminates inversion symmetry, which is a prerequisite for second-order nonlinear optical (NLO) effects[15] including second harmonic generation (SHG).[16–18] On the other hand, enantiomeric metal halides exhibit fascinating chiroptical activity[19,20] and chiral-induced spin selectivity (CISS).[21,22] Here, we reported the chiral zinc-based halides *via* introducing the organic ligands (*R*)-(−)/(*S*)-(+)-2-methylpiperazine (abbreviated as *R*-/*S*-MP). The NLO properties of the chiral zinc halides have been explored, whose SHG response is 19.6 times that of Z-cut quartz at 480 nm. Moreover, the successful alloying of Sb³⁺ into chiral zinc halide hosts results in the generation of circularly polarized luminescence (CPL) from self-trapped excitons (STEs). Accordingly, a quantum yield of 34.5% and luminescence dissymmetry factor (g_{lum}) of 1.81×10^{-3} can be achieved for the 10% Sb feeding.

A pair of chiral zinc halides are prepared *via* slow evaporation from their corresponding hydrochloric acid solutions. Single-crystal X-ray diffraction (SCXRD) analyses confirm that *R*-/*S*-2-MP-ZnCl crystalizes in the monoclinic $P2_1$ space group. Within their inorganic structural units, a tetrahedron is constructed by four Cl⁻ anions coordinated with a Zn²⁺ cation. The incorporation of a chiral amine isolates each tetrahedron, forming the typical zero-dimensional (0D) Zn-based halide.[23] Simultaneously, the chiral ligands also transfer the original chirality to the inorganic block buildings, successfully constructing the hybrid zinc halide enantiomer (Fig. 1a). As depicted in Fig. 1b and c, the as-synthesized chiral zinc halides display a colourless bar-like shape. The optical microscope pictures of the obtained samples indicate the orderly growth of the crystals. Powder XRD patterns of the two chiral Zn-based halides all present sharp peaks, and are in good agreement with the simulated results, implying high crystallinity and phase purity.[24]
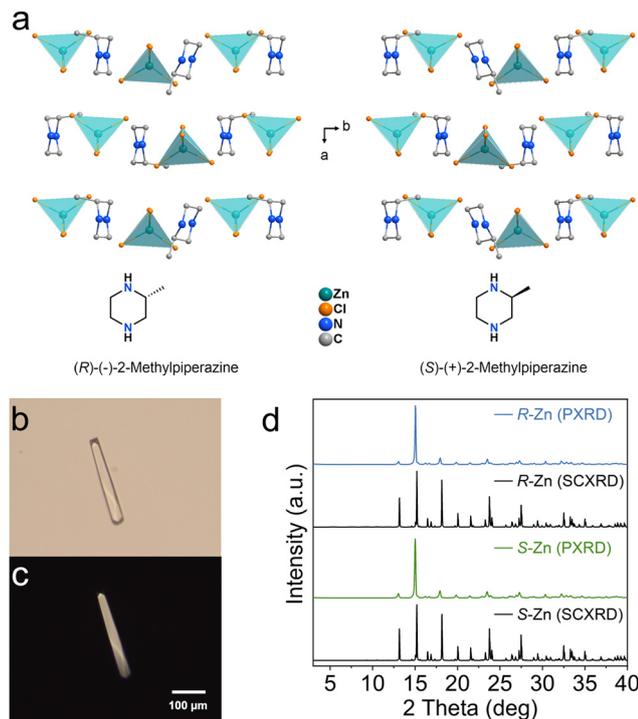
Fig. 1 (a) Crystal structures of **R-** and **S-Zn**. (b) Optical microscope image and (c) the corresponding crossing polarized microscope image of an **R-Zn** crystal. (d) Powder XRD patterns of **R-** and **S-Zn**.

Fig. 2 (a) UV-vis-NIR transmittance spectra of **R-/S-Zn**. (b) Wavelength-dependent SHG intensities of **R-Zn** at various excitation wavelengths from 800 to 1040 nm. (c) Polarization dependence of the SHG intensity from the **R-Zn** crystal under the excitation of 960 nm. (d) Logarithmic plot of SHG intensity as a function of the incident power.

Chiral spacer cations, $(R-/S-2-MP)^{2+}$, have been successfully incorporated, forming an enantiomeric pair of chiral zinc halides with acentric architectures. Induced by N–H···Cl–Zn hydrogen bonds, inorganic $(ZnCl_4)^{2-}$ tetrahedra engender the corresponding asymmetric tilts or distortions (Fig. S1, ESI†).[25,26] The chirality-induced asymmetric materials are generally employed to study second-order NLO features such as SHG.[27–30] As indicated in Fig. 2a, the $(R-/S-2-MP)ZnCl_4$ (abbreviated as **R-/S-Zn**) can both showcase a wide transparency window, retaining 70% optical transparency spanning from 0.5 to 2.5 μm.[31] The NLO signals of chiral zinc halides have been collected in reflection geometry *via* a home-built microscope equipped with a femtosecond pulsed laser (100 fs, 80 MHz). The wavelength-dependent SHG characterizations have been conducted at the same incident power by switching the pump wavelengths from 800 to 1040 nm at 20 nm intervals. Chiral zinc halide **R-Zn** manifests clear SHG responses in a wide wavelength range, especially at the excitation of 960 nm. Polarization dependent measurements of the NLO response of **R-Zn** at 480 nm have been carried out. Fig. 4c illustrates that the polarization plots agree well with the $\cos^4\theta$ function[32] with the maximum SHG intensity at polarized angles of 20 and 200 deg. The corresponding polarization ratio, $\rho = (I_{max} - I_{min})/(I_{max} + I_{min})$, is derived to be 97.7% for the *p*-analyzer, indicating the high anisotropy of the NLO responses. Analysis of the power-dependent SHG spectra (Fig. 2d) pumped at 960 nm unveils a quadratic dependence for the power-SHG intensity function, confirming the two-photon nature of the second-order NLO effect. Furthermore, the quadratic dependence on laser power can be retained until the incident power exceeds 575.0 mW. Thus, the laser damage
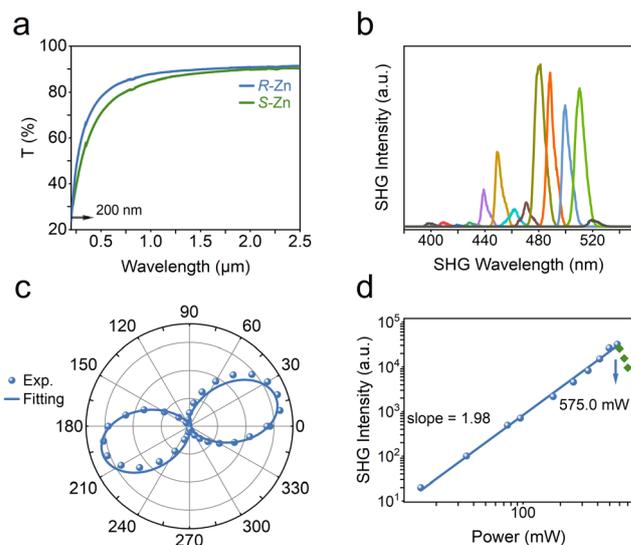
threshold (LDT) of **R-Zn** is estimated to be ~ 2.29 mJ cm^{-2} in pump fluence, given the laser spot of ~ 20 μm in diameter (100 fs, 80 MHz). In addition, the SHG efficiency of **R-Zn** has been evaluated *via* utilizing the Z-cut quartz as the benchmark. The obtained SHG response of **R-Zn** is 19.6 times that of Z-cut quartz at the optimized pump wavelength (Fig. S3, ESI†).

Numerous chiral metal halides have been utilized for NLOs and the detection of circularly polarized emission. However, many of these compounds demonstrate negligible photoluminescence (PL) at room temperature.[33] For the majority of zinc halides, luminescence is scarcely observed owing to its completely filled d10 electron configuration, which makes it difficult for Zn^{2+} ions to participate in luminescence processes.[34] The **R-Zn** and **S-Zn** are indeed non-luminescent at ambient temperature, as shown in Fig. S11 (ESI†). To improve this, doping strategies based on metal ions have been explored, particularly with 5s^2 metal ions (Sb^{3+}, Sn^{2+}, Bi^{3+}, *etc.*).[35,36] In this study, various amounts of Sb^{3+} have been then introduced into the chiral zinc chloride host. The powder XRD patterns (Fig. S4, ESI†) demonstrate that the **R-Zn:x%Sb** preserve the original undoped phase if the Sb^{3+} feeding concentration is less than 30%; otherwise, the $(R-2-MP)SbCl_5$ (abbreviated as **R-Sb**) phase replaces **R-Zn** as the dominant phase. For the structure of **R-Sb** (CCDC 803026[37]), a tetrahedron $(SbCl_4)^-$ with a free Cl^- constitutes each 0D inorganic unit. Moreover, when the Sb feeding level is less than 30%, as the feeding level increases, the diffraction peak shifts slightly to lower angles, indicating that the doping of Sb^{3+} ions ($r = 0.74$ Å, CN = 4) with a larger atomic radius than that of Zn^{2+} ($r = 0.60$ Å, CN = 4) ions causes lattice expansion.[38]

UV-vis diffuse reflection absorption spectra have been conducted to investigate the photophysical features of **R-Zn:x%Sb**. With increasing the Sb^{3+} feeding level, the absorption intensity

between 230–350 nm rises up significantly along with a bathochromic-shift of the absorption edge. The X-ray photo-electron spectra (XPS) testify the successful incorporation of Sb^{3+} into the chiral zinc halide host (Fig. S5, ESI†), as evidenced by the peaks at 539.8 and 530.4 eV, attributed to the Sb(III) $3d_{3/2}$ and $3d_{5/2}$ orbitals.[39] Thermogravimetric analysis (TGA) curves indicate that **R-Zn:x%Sb** are thermally stable up to 240 °C (Fig. S6, ESI†). After alloying Sb^{3+} ions, the PL spectra unveil broadband emission at around 616 nm with large Stokes shift for **R-Zn:x%Sb** (Fig. S7a, ESI†). However, no emission can be observed for **R-Sb** at room temperature, excluding the effect of impurities on the PL process. Time-resolved photoluminescence spectra indicate that **R-Zn:10%Sb** features a lifetime of 7.5 μs with a single exponential decay at the excitation of 350 nm (Fig. S7b, ESI†). This is consistent with the characteristics of self-trapped exciton (STE) emission.[39–41]

To validate the nature of the STE emission, varied-temperature PL measurements of **R-Zn:10%Sb** have been carried out (Fig. 3b). The emission band at 509 nm gradually emerges when the ambient temperature drops below 240 K. Meanwhile, as presented in Fig. S8 (ESI†), the emission intensity at 616 nm rises up while its full width at half-maximum (FWHM) narrows as the temperature declines, implying the enhanced radiative recombination from less phonon-exciton coupling.[42,43] The lifetimes (Fig. 3c) of **R-Zn:10%Sb** at 509 and 657 nm are confirmed to be 6.2 ns and 9.4 μs, conforming to the features of singlet ($^1P_1$) and triplet ($^3P_1$) STEs.[44] The excitation-emission mapping pattern of **R-Zn:10%Sb** at 80 K (Fig. S9, ESI†) shows that the peak at 509 nm is only observed at the short excitation wavelengths (<340 nm), revealing that the dual-emission stems from the various excited states. Modulating the doping ratio of Sb^{3+} in the zinc halide host offers a facile pathway to optimize their emission efficiency. In this study, a maximum photoluminescence quantum yield (PLQY) of

34.5% could be obtained for **R-Zn:10%Sb** by alternating the dopant ratio. However, excessive Sb content has been found to quench the original luminescence (Fig. 3d).

This chiral framework not only eliminates the spatial symmetry in the metal halide, but also facilitates chiral optical activity. The chiroptical performance of **R-/S-Zn:10%Sb** has been examined by circular dichroism (CD). The two chiral enantiomeric zinc halides present nearly reverse CD signals (Fig. 4a) at the same location between 300 and 600 nm on account of the Cotton effect, suggesting the chirality transfer from chiral organic ligands to achiral inorganic skeletons.[45,46] Moreover, the **R-/S-Zn:10%Sb** reveal clear mirror-image outlines for the CPL spectra (Fig. 4b), where the derived luminescent asymmetry factor (g_{lum}) values have been determined to be 1.81×10^{-3} for **R-Zn:10%Sb** and -1.43×10^{-3} for **S-Zn:10%Sb** at 616 nm, respectively.

A possible photoexcited emission process in **R-Zn:10%Sb** has been illustrated in Fig. 4d. Upon excitation by high-energy photons (330 nm), electrons will enter the singlet STE state. Then, partial electrons transfer to the triplet STE state via intersystem crossing (ISC).[44,47] Thus, both the 509 and 616 nm bands can be observed. However, the band at 509 nm only appears at low temperatures. Excitation by low-energy photons (351 nm) directly shifts the electrons to the triplet STE state and back to the ground state, resulting in the broadband emission solely at 616 nm.[48]

In summary, a pair of chiral zinc chlorides have been fabricated via introducing chiral organic cations into the system. Grounded on a noncentrosymmetric framework, the **R-Zn** crystals exhibit clear NLO responses, with an SHG intensity 19.6 times that of Z-cut quartz. Furthermore, melding trivalent antimony (Sb^{3+}) ions with $5s^2$ lone pair electrons into the **R-Zn** host can activate CPL, with a PLQY of 34.5% and a g_{lum} of 1.81×10^{-3}. Relevant PL measurements argue that the broadband emission originates
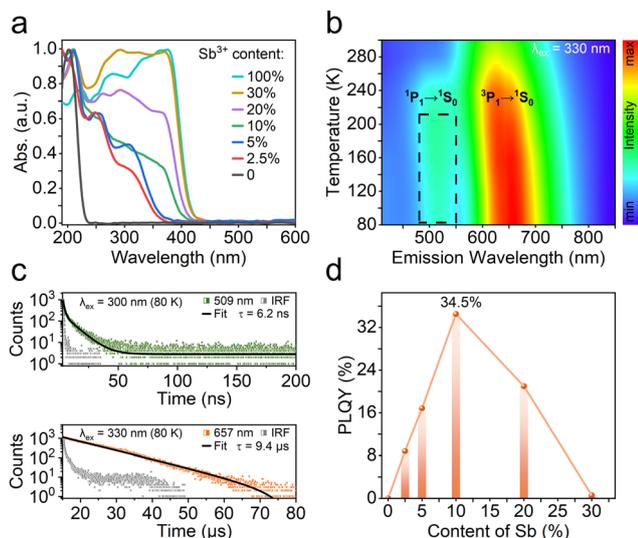

Fig. 3 (a) UV-vis absorption spectra, (b) varied-temperature PL spectra of **R-Zn:10%Sb** at excitation of 330 nm, (c) PL decay profiles of 509 and 657 nm at 80 K for **R-Zn:10%Sb**, and (d) quantum yield of **R-Zn:x%Sb** with various Sb^{3+} dopant amounts.
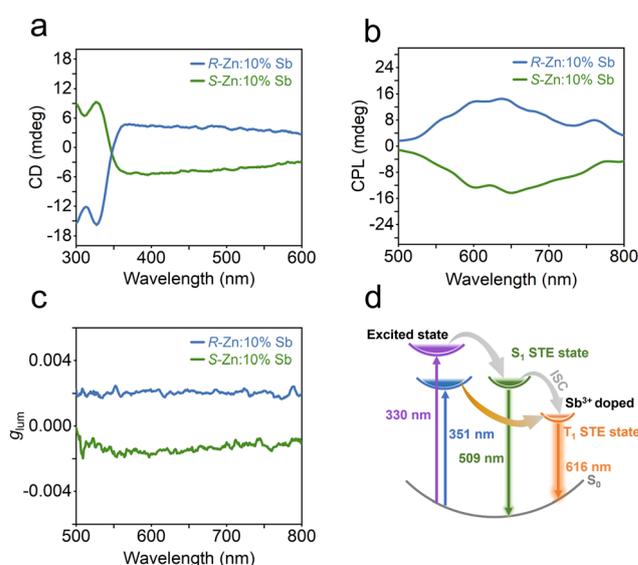

Fig. 4 (a) CD spectra, (b) CPL spectra and (c) corresponding g_{lum} of **R-/S-Zn:10%Sb**. (d) Schematic illustration of the proposed PL process in **R-Zn:x%Sb**.

from the STEs. This work offers a novel channel to design and manufacture second-order NLO materials and CPL material emitters based on low-dimensional chiral metal halides.

Conflicts of interest

There are no conflicts to declare.

Notes and references

1 S. P. Rodrigues, S. Lan, L. Kang, Y. Cui, P. W. Panuski, S. Wang, A. M. Urbas and W. Cai, *Nat. Commun.*, 2017, **8**, 14602.
2 S. Mondal, F. Dumur, D. Gigmes, M. P. Sibi, M. P. Bertrand and M. Nechab, *Chem. Rev.*, 2022, **122**, 5842–5976.
3 S. Tashiro and M. Shionoya, *Acc. Chem. Res.*, 2020, **53**, 632–643.
4 C. Zhang, S. Li, X.-Y. Dong and S.-Q. Zang, *Aggregate*, 2021, **2**, e48.
5 H. Hübener, U. De Giovannini, C. Schäfer, J. Andberger, M. Ruggenthaler, J. Faist and A. Rubio, *Nat. Mater.*, 2021, **20**, 438–442.
6 D. E. Kharzeev and J. Liao, *Nat. Rev. Phys.*, 2021, **3**, 55–63.
7 Y. Wang, J. Xu, Y. Wang and H. Chen, *Chem. Soc. Rev.*, 2013, **42**, 2930–2962.
8 A. Younis, C.-H. Lin, X. Guan, S. Shahrokhi, C.-Y. Huang, Y. Wang, T. He, S. Singh, L. Hu, J. R. D. Retamal, J.-H. He and T. Wu, *Adv. Mater.*, 2021, **33**, 2005000.
9 C. Zhou, H. Lin, Q. He, L. Xu, M. Worku, M. Chaaban, S. Lee, X. Shi, M.-H. Du and B. Ma, *Mater. Sci. Eng., R*, 2019, **137**, 38–65.
10 H. Duim and M. A. Loi, *Matter*, 2021, **4**, 3835–3851.
11 Z. Guo, J. Li, R. Chen and T. He, *Prog. Quantum Electron.*, 2022, **82**, 100375.
12 D. G. Billing and A. Lemmerer, *Acta Crystallogr., Sect. E: Struct. Rep. Online*, 2003, **59**, m381–m383.
13 J. Ma, H. Wang and D. Li, *Adv. Mater.*, 2021, **33**, 2008785.
14 J. Crassous, M. J. Fuchter, D. E. Freedman, N. A. Kotov, J. Moon, M. C. Beard and S. Feldmann, *Nat. Rev. Mater.*, 2023, DOI: **10.1038/s41578-023-00543-3**.
15 X. Han, F. Ge, J. Xu and X.-H. Bu, *Aggregate*, 2021, **2**, e28.
16 C. Yuan, X. Li, S. Semin, Y. Feng, T. Rasing and J. Xu, *Nano Lett.*, 2018, **18**, 5411–5417.
17 X. Fu, Z. Zeng, S. Jiao, X. Wang, J. Wang, Y. Jiang, W. Zheng, D. Zhang, Z. Tian, Q. Li and A. Pan, *Nano Lett.*, 2023, **23**, 606–613.
18 Y. Peng, X. Liu, L. Li, Y. Yao, H. Ye, X. Shang, X. Chen and J. Luo, *J. Am. Chem. Soc.*, 2021, **143**, 14077–14082.
19 X. Li, F. Wu, Y. Yao, W. Wu, C. Ji, L. Li, Z. Sun, J. Luo and X. Liu, *J. Am. Chem. Soc.*, 2022, **144**, 14031–14036.
20 X. Ji, S. Geng, S. Zhang, Y. Gong, X. Zhang, R. Li, Y. Liu, J. Chen, R. Chen, Z. Xiao and L. Mao, *Chem. Mater.*, 2022, **34**, 8262–8270.
21 H. Lu, Z. V. Vardeny and M. C. Beard, *Nat. Rev. Chem.*, 2022, **6**, 470–485.
22 R. Naaman, Y. Paltiel and D. H. Waldeck, *Acc. Chem. Res.*, 2020, **53**, 2659–2667.
23 X. Liu, C. Peng, L. Zhang, D. Guo and Y. Pan, *J. Mater. Chem. C*, 2022, **10**, 204–209.
24 L. Wang, Y. Xue, M. Cui, Y. Huang, H. Xu, C. Qin, J. Yang, H. Dai and M. Yuan, *Angew. Chem., Int. Ed.*, 2020, **59**, 6442–6450.
25 L. Yao, Z. Zeng, C. Cai, P. Xu, H. Gu, L. Gao, J. Han, X. Zhang, X. Wang, X. Wang, A. Pan, J. Wang, W. Liang, S. Liu, C. Chen and J. Tang, *J. Am. Chem. Soc.*, 2021, **143**, 16095–16104.
26 J.-H. Lee, N. C. Bristowe, J. H. Lee, S.-H. Lee, P. D. Bristowe, A. K. Cheetham and H. M. Jang, *Chem. Mater.*, 2016, **28**, 4259–4266.
27 Q. Wen, S. Tenenholtz, L. J. W. Shimon, O. Bar-Elli, L. M. Beck, L. Houben, S. R. Cohen, Y. Feldman, M. Oron, M. Lahav and M. E. van der Boom, *J. Am. Chem. Soc.*, 2020, **142**, 14210–14221.
28 Q. Qian, R. Zu, Q. Ji, G. S. Jung, K. Zhang, Y. Zhang, M. J. Buehler, J. Kong, V. Gopalan and S. Huang, *ACS Nano*, 2020, **14**, 13333–13342.
29 Z. Guo, J. Li, J. Liang, C. Wang, X. Zhu and T. He, *Nano Lett.*, 2022, **22**, 846–852.
30 Z. Yu, S. Cao, Y. Zhao, Y. Guo, M. Dong, Y. Fu, J. Zhao, J. Yang, L. Jiang and Y. Wu, *ACS Appl. Mater. Interfaces*, 2022, **14**, 39451–39458.
31 J. Chen, H. Chen, F. Xu, L. Cao, X. Jiang, S. Yang, Y. Sun, X. Zhao, C. Lin and N. Ye, *J. Am. Chem. Soc.*, 2021, **143**, 10309–10316.
32 Y. Zheng, X. Han, P. Cheng, X. Jia, J. Xu and X.-H. Bu, *J. Am. Chem. Soc.*, 2022, **144**, 16471–16479.
33 Z. Wang, X. Wang, Z. Chen, Y. Liu, H. Xie, J. Xue, L. Mao, Y. Yan and H. Lu, *Angew. Chem., Int. Ed.*, 2022, **62**, e202215206.
34 E. Merzlyakova, S. Wolf, S. Lebedkin, L. Bayarjargal, B. L. Neumeier, D. Bartenbach, C. Holzer, W. Klopper, B. Winkler, M. Kappes and C. Feldmann, *J. Am. Chem. Soc.*, 2021, **143**, 798–804.
35 Y. Wei, C. Li, Y. Li, Z. Luo, X. Wu, Y. Liu, L. Zhang, X. He, W. Wang and Z. Quan, *Angew. Chem., Int. Ed.*, 2022, **61**, e202212685.
36 W. Zhang, W. Zheng, L. Li, P. Huang, Z. Gong, Z. Zhou, J. Sun, Y. Yu and X. Chen, *Angew. Chem., Int. Ed.*, 2022, **61**, e202116085.
37 L. Li and G.-X. Wang, *Acta Crystallogr., Sect. E: Struct. Rep. Online*, 2010, **66**, m1629.
38 Y. Dai, Q. Wei, T. Chang, J. Zhao, S. Cao, B. Zou and R. Zeng, *J. Phys. Chem. C*, 2022, **126**, 11238–11245.
39 B. Su, M. Li, E. Song and Z. Xia, *Adv. Funct. Mater.*, 2021, **31**, 2105316.
40 Q. Guo, X. Zhao, B. Song, J. Luo and J. Tang, *Adv. Mater.*, 2022, **34**, 2201008.
41 V. Pinchetti, F. Moro, B. Zhang, M. Fanciulli, L. De Trizio, F. Meinardi, L. Manna and S. Brovelli, *ACS Energy Lett.*, 2022, **7**, 1566–1573.
42 L. Li and Z. Xia, *Chem. Soc. Rev.*, 2021, **50**, 2626–2662.
43 L. Zhou, L. Zhang, H. Li, W. Shen, M. Li and R. He, *Adv. Funct. Mater.*, 2021, **31**, 2108561.
44 J.-H. Wei, J.-F. Liao, L. Zhou, J.-B. Luo, X.-D. Wang and D.-B. Kuang, *Sci. Adv.*, 2021, **7**, eabg3989.
45 S. Ma, J. Ahn and J. Moon, *Adv. Mater.*, 2021, **33**, 2005760.
46 S. Ma, Y.-K. Jung, J. Ahn, J. Kyhm, J. Tan, H. Lee, G. Jang, C. U. Lee, A. Walsh and J. Moon, *Nat. Commun.*, 2022, **13**, 3259.
47 C. Sun, Z. Deng, Z. Li, Z. Chen, X. Zhang, J. Chen, H. Lu, P. Canepa, R. Chen and L. Mao, *Angew. Chem., Int. Ed.*, 2023, **62**, e202216720.
48 J. Wu, X. Li, X. Lian, B. Su, J. Pang, M.-D. Li, Z. Xia, J. Z. Zhang, B. Luo and X.-C. Huang, *ACS Nano*, 2021, **15**, 15354–15361.